Daily to Decadal Sea Surface Temperature Variability Driven by State-Dependent Stochastic Heat Fluxes

Philip Sura, Matthew Newman, and Michael Alexander

NOAA-CIRES Climate Diagnostics Center, Boulder, Colorado

March 10, 2006

Accepted for publication in *Journal of Physical Oceanography*

Corresponding author address:
Philip Sura
NOAA-CIRES Climate Diagnostics Center, R/CDC1
325 Broadway, Boulder, CO 80305-3328
Phone: (303) 497-4426, Fax: (303) 497-6449
E-Mail: Philip.Sura@noaa.gov

Abstract

The classic Frankignoul-Hasselmann hypothesis for sea surface temperature (SST) variability of an oceanic mixed layer assumes that the surface heat flux can be simply parameterized as noise induced by atmospheric variability plus a linear temperature relaxation rate. It is suggested here, however, that rapid fluctuations in this rate, as might be expected for example due to gustiness of the sea surface winds, are large enough that they cannot be ignored. Such fluctuations cannot be fully modeled by noise that is independent of the state of the SST anomaly itself. Rather, they require the inclusion of a state-dependent (that is, multiplicative) noise term, which can be expected to impact both persistence and the relative occurrence of high amplitude anomalies.

As a test of this hypothesis, daily observations at several Ocean Weather Stations (OWS) are examined. Significant skewness and kurtosis of the distributions of SST anomalies is found, which is shown to be consistent with a multiplicative noise model. The observed wintertime SST distribution at OWS P is reproduced using a single column variable depth mixed layer model; the resulting non-Gaussianity is found to be largely due to the state-dependence of rapidly-varying (effectively stochastic) sensible and latent heat flux anomalies.

Our model for the non-Gaussianity of anomalous SST variability (counterintuitively) implies that the multiplicative noise increases the persistence, predictability, and variance of midlatitude SST anomalies. The effect is strongest on annual and longer timescales and may, therefore, be important to understand and model interannual and interdecadal SST and related climate variability.

1 Introduction

The typical timescale of atmospheric variability is considerably shorter than the typical timescale of sea surface temperature (SST) variability. As a result, the effect of atmospheric forcing of SST anomalies T'_o can be represented by a simple stochastic model of the oceanic mixed layer,

$$\frac{dT'_o}{dt} = -\lambda T'_o + \xi \tag{1}$$

(Hasselmann 1976; Frankignoul and Hasselmann 1977, hereafter FH), where λ is a rate coefficient representing the transfer of heat from the slowly evolving mixed layer heat anomaly, and ξ is Gaussian white-noise representing surface heat fluxes due to rapidly varying weather fluctuations. The e-folding timescale of SST variability is thus $\tau = 1/\lambda$. Such a simple univariate linear system has been surprisingly successful in describing much of the variability of anomalous midlatitude SSTs (e.g., Frankignoul and Hasselmann 1977; Reynolds 1978; Blaauboer et al. 1982; Hall and Manabe 1997).

This classical stochastic view implies that SST anomalies obey a Gaussian distribution. Indeed, *monthly averaged* SST anomalies are nearly Gaussian. Yet we might expect them to be Gaussian because of the Central Limit Theorem (e.g., Gardiner 2004; Paul and Baschnagel 1999), i.e., the Gaussianity may be due solely to the averaging procedure and not to any particular dynamical process. In fact, as we will show, observations from Ocean Weather Stations (OWSs) reveal that Probability Distribution Functions (PDFs) of *daily averaged* SST anomalies are actually significantly non-Gaussian.

The presence of non-Gaussianity suggests the possible importance of nonlinearity to the

evolution of SST anomalies, appearing to contradict the FH paradigm. However, if this nonlinearity also acts on a very short timescale, then the FH paradigm may only require a small adjustment. Suppose the linear coefficient in (1) contains a rapidly varying component; that is, $\lambda = \langle\lambda\rangle + \lambda'$, where $\langle\lambda\rangle$ is constant but λ' varies rapidly; note that the time mean of λ' is zero. Such rapid fluctuations in the feedback coefficient might be expected, for example, if it has a dependence upon not just a constant or slowly varying wind speed, but also upon the gustiness of the winds. Then we might also approximate λ' as white-noise. However, unlike the noise term ξ which is independent of T_o', a stochastically fluctuating λ' would result in a second noise term $\lambda' T_o'$ which depends upon the SST anomaly itself. This state-dependent noise is also known as multiplicative noise. A system driven with such multiplicative noise has two characteristics of interest here. First, in general it will have a non-Gaussian PDF, even though the deterministic portion of (1) is linear. Second, although the autocorrelation function for T_o' remains an exponential, the multiplicative noise acts to effectively increase the time scale τ through a phenomenon known as noise-induced drift, which occurs because the time mean of the multiplicative noise term, $\langle\lambda' T_o'\rangle$, is not zero. For a mathematically more advanced discussion, see, for example, Gardiner (2004); Kloeden and Platen (1992), and see Sardeshmukh et al. (2001) and Penland (2003a,b) for related discussions focusing on climate dynamics.

In this paper we present a simple univariate stochastic model of midlatitude SST anomalies that accounts for rapid fluctuations in surface heat fluxes, such as might result from the gustiness of sea surface winds. The parameters of this model are determined from OWS data whose non-Gaussian PDFs are described in section 2. In section 3 we justify a noise

component of λ through a scale analysis of wind-driven surface heat flux, as parameterized by simple heat flux bulk formulae. This hypothesis is then explored and quantified using two complementary approaches. First, in section 4 we use both linear and nonlinear inverse methods to estimate stochastic models from data. The nonlinear model is additionally used to examine the impact of multiplicative noise on the persistence and low-frequency variability of SST anomalies. Second, in section 5 we show that the non-Gaussianity of observed anomalous SST variability during the extended winter season at OWS P can be reproduced by a single column variable-depth mixed layer model, and that it is the multiplicative noise nature of the surface heat fluxes that is responsible for this non-Gaussianity. Finally, section 6 provides a summary and discussion.

2 PDFs of daily Averaged SST

To re-examine the effect of stochastic weather fluctuations on anomalous SSTs, we first analyze the PDFs of daily averaged SST anomalies obtained from Ocean Weather Station records [see Dinsmore (1996) for a brief history of Ocean Weather Stations and Diaz et al. (1987) for climatological summaries]. Table 1 lists the stations analyzed, their locations, and the time periods of data availability. We restrict our study to locations where univariate linear stochastic theory provides a good fit to observed anomalous SST variability: P, N, and V in the North Pacific, and K in the North Atlantic (Hall and Manabe 1997).

2.1 Data

Daily SST anomalies were determined as follows. First, daily averages were calculated from the raw 3-hourly data. Then the climatological monthly averages were estimated. A daily climatology was constructed by linear interpolation using these monthly averages as base points. Finally, daily anomalies were calculated by subtracting the daily climatology from the mean daily values.

We analyzed the resulting full-year SST anomaly timeseries. To account for possible effects of the annual cycle we analyzed extended summer (May-October) and extended winter (November-April) subsets as well.

2.2 Probability Density Functions

PDFs are a useful measure to examine the dynamics of stochastic systems. In particular, deviations from Gaussianity, or anomalous statistics, can shed light on the underlying dynamics (e.g., Peinke et al. 2004; Sura et al. 2005). PDFs can be estimated using different techniques. The easiest way is to calculate the normalized histogram by binning the data. This is a non-parametric method because no assumptions are made of the functional form of the PDF. Non-parametric methods are normally used as a reliable first-order PDF estimate when there is no reasonable physical justification for a particular distribution. For a parametric estimation of a PDF one specifies the functional form of the PDF in advance, and the parameters of the PDF are then determined by a Maximum Likelihood Estimate (MLE). The parametric distribution we use is the skew t-distribution, a skewed and kurtosed

alternative to the normal distribution which is capable of adapting very closely to skewed and heavy-tailed data (Azzalini and Capitanio 2003; Jones and Faddy 2003). We use both methods here.

In the following section, all discussed deviations from Gaussianity are significant at least at the 95% confidence level, with large amplitude deviations significant at the 99% confidence level, as determined by the Monte-Carlo method employed in, e.g., Sura et al. (2005).

2.3 Ocean Weather Station P

Of all the Ocean Weather Stations, OWS P may be best suited for linear univariate stochastic theory (Hall and Manabe 1997). It has a long high-quality record, the El Niño-Southern Oscillation (ENSO) signal is relatively weak there (e.g., Alexander et al. 2002), and it is located far from strong currents.

The PDFs of full-year daily SST anomalies, related Gaussian distributions, and anomalies (deviations from Gaussianity) at OWS P are shown in Fig. 1. In Fig. 1a the PDF (steps) is calculated as a normalized histogram, whereas in Fig. 1b the PDF (solid line) is calculated as a MLE to a skew t-distribution. Comparison in either case to the related Gaussian distribution (dashed lines) shows that the PDF has a strong peak, weak flanks, and heavy tails relative to a Gaussian distribution (i.e., the PDF is kurtosed). Furthermore, the PDF is slightly skewed. The skew t-distribution captures all the important features of the histogram: the strong peak, weak flanks, heavy-tails, and the skew.

2.4 Other Ocean Weather Stations

Hall and Manabe (1997) have shown that while over most of the world ocean anomalous SST variability is consistent with the simple FH model, there are a few regions where this stochastic theory cannot be applied. Near strong boundary currents like the Gulf Stream and the Kuroshio (and both their extensions, the North Atlantic and the North Pacific currents) mesoscale eddies enhance SST variability at high-frequencies. Furthermore, in the northern North Atlantic, large scale variations of the thermohaline ocean circulation are responsible for much of the low-frequency variations. And, of course, regions with sea-ice are excluded as well.

After analyzing data from the remaining stations, we find that, in agreement with Hall and Manabe (1997), there are four stations with long records where the autocorrelation functions (and the spectra) can be modeled with univariate red noise: P, N, and V in the North Pacific, and K in the North Atlantic. These stations are all in midlatitudes and far away from strong currents. The PDFs (full year, extended summer and winter) of SST anomalies at these stations are shown in Fig. 2 (we only show the skew t-distributions; the histograms have a similiar shape). The PDFs at OWSs K and N are qualitatively similar to the PDF at OWS P (Fig. 1), although their deviations from Gaussianity are somewhat larger. OWS V shows a slightly different behavior: the PDFs have similar kurtosis as the other stations, but the skew has the opposite sign. In all cases, similar deviations from Gaussianity is present in both the winter and summer subsets.

To summarize, the non-Gaussianity at OWS P is not unique but a general feature at

OWSs where linear stochastic theory can be applied. Furthermore, the non-Gaussianity does not appear strongly seasonally dependent, suggesting that the full-year daily SST anomaly record can be used to study anomalous SST variability [as in Hall and Manabe (1997)].

3 Extending the Frankingnoul-Hasselmann Null Hypothesis

In the previous section, we examined ocean stations whose daily SST data are consistent with univariate stochastic theory and yet obey a non-Gaussian distribution. This immediately suggests the possible importance of multiplicative noise. As an initial exploration of this issue, we next consider a straightforward extension of the classic FH stochastic SST anomaly model, in which we add a stochastic process resulting from rapidly fluctuating wind speeds to the constant feedback coefficient.

3.1 The basic mixed layer equations

The simplest model for midlatitude SSTs assumes a well mixed and horizontally homogeneous layer of constant depth h and temperature T_o in contact with the overlying atmosphere, but isolated from the layers below the thermocline. For the sake of simplicity, all effects of horizontal advection and salinity are ignored as well. Then the local heat budget equation can be written as (see, e.g. Frankignoul and Hasselmann 1977)

$$\frac{dT_o}{dt} = \frac{f(T_o, T_a, q, |\mathbf{U}|, R)}{h} \quad , \tag{2}$$

where f denotes the total heat flux through the air-sea interface, which depends on the SST T_o, air temperature T_a, humidity q, wind speed $|\mathbf{U}|$, and the net radiation R. Neglecting the radiation flux, the bulk formula for the heat flux f is

$$f \approx \frac{\rho_a C_a}{\rho_w C_w} C_H (1+B)(T_a - T_o)|\mathbf{U}| \quad , \tag{3}$$

where C_H is the bulk transfer coefficient of the latent and sensible heat flux, B is the inverse Bowen ratio (ratio of latent to sensible heat flux), ρ_w and ρ_a are the densities of sea-water and air, and C_w and C_a are the specific heats (at constant pressure) of sea-water and air.

For small temperature anomalies ΔT_o and ΔT_a a Taylor expansion of the heat flux f yields

$$\frac{d}{dt}(\langle T_o \rangle + \Delta T_o) = \frac{1}{h}\left[f(\langle T_o \rangle, \langle T_a \rangle) + \frac{\partial f}{\partial T_o}\Big|_{\langle T_o \rangle} \Delta T_o + \frac{\partial f}{\partial T_a}\Big|_{\langle T_a \rangle} \Delta T_a \right] \quad . \tag{4}$$

Assuming that the evolution of the mean temperature $\langle T_o \rangle$ is balanced by the time mean of $f(\langle T_o \rangle, \langle T_a \rangle) = \langle f \rangle(\langle T_o \rangle, \langle T_a \rangle) + f'(\langle T_o \rangle, \langle T_a \rangle)$, that is $d\langle T_o \rangle/dt = \langle f \rangle(\langle T_o \rangle, \langle T_a \rangle)/h$, and defining $\Delta T_o \equiv T_o'$ and $\Delta T_a \equiv T_a'$ the equation for the SST anomaly T_o' becomes:

$$\frac{dT_o'}{dt} = \frac{f'(\langle T_o \rangle, \langle T_a \rangle)}{h} + \frac{1}{h}\frac{\partial f}{\partial T_o}\Big|_{\langle T_o \rangle} T_o' + \frac{1}{h}\frac{\partial f}{\partial T_a}\Big|_{\langle T_a \rangle} T_a' \quad . \tag{5}$$

FH ignored variations in T_a. To include atmospheric variability in a simple manner, we note that on long time scales T_a' equilibrates with T_o' (e.g., Barsugli and Battisti 1998); even on daily time scales, at OWS P the correlation between T_a' and T_o' is 0.67. A simple relation for atmospheric variability is thus the regression equation

$$T_a' = \alpha T_o' + \xi' \tag{6}$$

where typically the remainder ξ' represents rapidly varying (on a 2-3 day timescale) noise. Then

$$\frac{dT_o'}{dt} = \frac{f'(\langle T_o \rangle, \langle T_a \rangle)}{h} + \frac{(1-\alpha)}{h}\frac{\partial f}{\partial T_o}\Big|_{\langle T_o \rangle} T_o' - \frac{1}{h}\frac{\partial f}{\partial T_o}\Big|_{\langle T_o \rangle} \xi' \quad . \tag{7}$$

As in FH variations in the inverse Bowen ratio B and the transfer coefficient C_H are ignored. That is, we assume that heat flux variability is only due to wind speed variability. This is a reasonable approximation in our simple framework, since heat flux anomalies are strongly related to wind speed anomalies (e.g., Ronca and Battisti 1997; Alexander and Scott 1997). This is not a perfect approximation, of course; as we will see in section 5, variations in these terms have an impact on the skewness, and by combining the sensible and latent heat fluxes together we obscure the latent heat flux dependence upon the dewpoint temperature. Furthermore, we neglect the correlation between T_a' and T_o' (i.e., $\alpha \equiv 0$). The important point is that these simplifications allow the following derivation to clearly establish the fundamental nature of the multiplicative noise.

The wind speed is split into a mean $\langle |\mathbf{U}| \rangle$ and a deviation from the mean $|\mathbf{U}|'$, so that the mean heat flux $\langle f \rangle$ depends upon $\langle |\mathbf{U}| \rangle$ and the heat flux deviation f' depends upon $|\mathbf{U}|'$. Then the anomalous heat flux f' and the heat flux derivative $\partial f / \partial T_o$ become

$$f'(\langle T_o \rangle, \langle T_a \rangle) = \frac{\rho_a C_a}{\rho_w C_w} C_H (1+B)(\langle T_a \rangle - \langle T_o \rangle)|\mathbf{U}|' \tag{8}$$

and

$$\frac{\partial f}{\partial T_o}\Big|_{\langle T_o \rangle} \equiv \left\langle \frac{\partial f}{\partial T_o} \right\rangle + \left(\frac{\partial f}{\partial T_o} \right)' = -\frac{\rho_a C_a}{\rho_w C_w} C_H (1+B) \left[\langle |\mathbf{U}| \rangle + |\mathbf{U}|' \right] \quad , \tag{9}$$

where $\partial f / \partial T_o$is split into a mean heat flux derivative $\langle \partial f / \partial T_o \rangle = -(\rho_a C_a)(\rho_w C_w)^{-1} C_H (1+$

$B)\langle|\mathbf{U}|\rangle$ and an anomalous heat flux derivative $(\partial f/\partial T_o)' = -(\rho_a C_a)(\rho_w C_w)^{-1} C_H(1+B)|\mathbf{U}|'$. Note that f' is a function of only $|\mathbf{U}|'$, whereas $\partial f/\partial T_o$ is a function of both $\langle|\mathbf{U}|\rangle$ and $|\mathbf{U}|'$.

3.2 Scaling the equation

To see if a multiplicative noise term is necessary, we first scale the terms in Eqs. (8) and (9). Using typical parameters for the conditions at OWS P (see Table 2) we obtain $f'/h = O(0.2\ \mathrm{K\,day^{-1}})$, $h^{-1}\langle\partial f/\partial T_o\rangle T_o' = O(0.1\ \mathrm{K\,day^{-1}})$, and $h^{-1}(\partial f/\partial T_o)'\, T_o' = O(0.05\ \mathrm{K\,day^{-1}})$. Note that the relative importance of $h^{-1}\langle\partial f/\partial T_o\rangle T_o'$ and $h^{-1}(\partial f/\partial T_o)'\, T_o'$ is solely determined by the ratio of the mean wind speed $\langle|\mathbf{U}|\rangle$ to the strength of the wind speed anomaly $|\mathbf{U}|'$. As this ratio is only about 2 to 1 throughout the midlatitude storm tracks (e.g., Monahan 2005b) the effect of wind fluctuations on SST anomalies may come through the variability of not only the anomalous heat flux f' but also the anomalous heat flux derivative $(\partial f/\partial T_o)'$.

3.3 Neglecting the anomalous heat flux derivative $(\partial \mathbf{f}/\partial \mathbf{T_o})'$: Modeling SST anomalies with additive noise

In the stochastic SST model introduced by FH, the anomalous heat flux derivative was neglected. The heat flux term f'/h [see Eq. (8)] is parameterized as Gaussian (additive) white-noise η [scaled by the parameter σ; see Eq. (10) below]. In other words, it is assumed that $|\mathbf{U}|'$ can be approximated by Gaussian white-noise. This assumption is reasonable since daily wind speed anomalies are almost uncorrelated and have a distribution that is nearly Gaussian. For example, at OWS P wind speed anomalies are almost uncorrelated after

2–3 days (Fig. 3a) and deviations from Gaussianity are relatively small (Fig. 3b). Then, treating the term $h^{-1}\partial f/\partial T_o$ [see Eq. (9)] as a constant parameter $\lambda = h^{-1}\langle \partial f/\partial T_o \rangle = -h^{-1}(\rho_a C_a)(\rho_w C_w)^{-1} C_H (1+B)\langle |\mathbf{U}| \rangle$, FH derived the familiar stochastic differential equation (SDE):

$$\frac{dT_o'}{dt} = -\lambda\, T_o' + \sigma\, \eta \quad , \tag{10}$$

with the Gaussian white-noise η satisfying $\langle \eta(t) \rangle = 0$ and $\langle \eta(t)\eta(t') \rangle = \delta(t-t')$. This is the SDE of a univariate Ornstein-Uhlenbeck process, also called damped Brownian motion. When λ is determined from observations, Eq. (10) results in the familiar red-noise spectrum of T_o' in close agreement with observations. However, the PDF of an Ornstein-Uhlenbeck process is strictly Gaussian and, therefore, not consistent with the results of section 2. Thus, the classical stochastic model of midlatitude SST variability should be improved to explain the non-Gaussianity of observed SST anomalies. Here we improve the stochastic model by including the anomalous heat flux derivative $(\partial f/\partial T_o)'$.

3.4 Including the anomalous heat flux derivative $(\partial \mathbf{f}/\partial \mathbf{T_o})'$: Modeling SST anomalies with multiplicative noise

The scaling analysis of section 3.2 suggests that $h^{-1}\partial f/\partial T_o$ should not be a constant parameter. Moreover, to be consistent $|\mathbf{U}|'$ should be a stochastic process both in Eqs. (8) and (9). That is, the anomalous heat flux derivative $(\partial f/\partial T_o)'$ is parameterized as multiplicative noise, since it is the product of a slowly varying quantity (T_o') and a rapidly varying quantity

($|\mathbf{U}|'$). Therefore, we replace the FH model (1) with the following SDE for T_o':

$$\frac{dT_o'}{dt} = -\lambda T_o' + \sqrt{2M}\, T_o' \eta_M + \sqrt{2D}\, \eta_D \tag{11}$$

with Gaussian white-noise satisfying

$$\langle \eta_M(t)\eta_M(t')\rangle = \delta(t-t') \ , \ \langle \eta_D(t)\eta_D(t')\rangle = \delta(t-t')\,. \tag{12}$$

D and M are constants governing the strength of the additive and multiplicative noise terms. Note that the actual noise amplitudes are $\sqrt{2D}$ and $\sqrt{2M}$; this definition is solely used for later mathematical convenience.

As was discussed in the introduction, multiplicative noise acts to lengthen the observed decorrelation timescale of T_o'. The autocorrelation function $\langle T_o'(t)T_o'(s)\rangle$ is given by (Sakaguchi 2001; Anteneodo and Tsallis 2003)

$$\langle T_o'(t)T_o'(s)\rangle = \frac{D}{\lambda - 2M} \exp\left(-(\lambda - M)|t-s|\right) \qquad . \tag{13}$$

As is the case with purely additive noise ($M = 0$), the autocorrelation decays exponentially. However, the decorrelation timescale is now $\tau = (\lambda - M)^{-1} = \lambda_{eff}^{-1}$. That is, the noise-induced drift is M, so that stronger multiplicative noise *increases* the persistence of midlatitude SST anomalies. The spectrum of SST anomalies $S(\omega)$ can be calculated by Fourier-transforming the autocorrelation function (13):

$$S(\omega) = \frac{D(\lambda - M)}{(\lambda - 2M)} \ \left(\omega^2 + (\lambda - M)^2\right)^{-1} \qquad . \tag{14}$$

In addition, the multiplicative noise acts to produce a non-Gaussian stationary PDF of T_o':

$$p(T_o') = \Theta(D + M{T_o'}^2)^{-\Pi} \tag{15}$$

(Sakaguchi 2001; Anteneodo and Tsallis 2003) where $\Pi = (\lambda_{eff} + 2M)/2M$. The normalization constant Θ is given by:

$$\Theta = \frac{M^{1/2} D^{\Pi - 1/2}}{\beta(1/2, \Pi - 1/2)} = \frac{M^{1/2} D^{\Pi - 1/2} \Gamma(\Pi)}{\Gamma(1/2)\Gamma(\Pi - 1/2)} \tag{16}$$

where $\beta(x, y)$ is the beta-function, and $\Gamma(x)$ is the gamma-function: $\beta(x, y) = \Gamma(x)\Gamma(y)/\Gamma(x + y)$. Having $p(T'_o)$ the moments of T'_o can be calculated. The first (mean) and the third moment (skew) are zero because the problem is symmetric with respect to $T'_o = 0$. The second moment (variance) is

$$\langle {T'_o}^2 \rangle \equiv \int_{-\infty}^{\infty} {T'_o}^2 p \, dT'_o = \frac{D}{\lambda_{eff} - M} \,, \tag{17}$$

and the fourth moment (kurtosis) is

$$\langle {T'_o}^4 \rangle \equiv \int_{-\infty}^{\infty} {T'_o}^4 p \, dT'_o = \frac{3D^2}{\lambda_{eff}^2 - 4\lambda_{eff} M + 3M^2} \,. \tag{18}$$

4 Inverse Stochastic Models of SST Anomalies

In the following we determine stochastic models for anomalous SST variability from data using inverse methods. First (in section 4.1) we estimate the parameters of the linear multiplicative noise model [Eq. (11)]. Second (in section 4.3) we estimate a more general nonlinear stochastic model from data to test the validity of the linear model. Furthermore, we use the nonlinear model to explore the impact of multiplicative noise on the predictability and the low-frequency variability of SST anomalies.

4.1 Linear inverse models

The parameters in Eq. (11) can be estimated from data by first determining the variance $\langle T_o'^2 \rangle$, the kurtosis $\langle T_o'^4 \rangle$, and the effective damping λ_{eff} from the observed autocorrelation function. Then M and D can be found from the two nonlinear (quadratic) equations [Eqs. (17) and (18)]. The parameters of the linear inverse models are summarized in Table 3.

The corresponding distributions $p(T_o')$ as defined by Eqs. (15) and (16) for full-year, extended winter and summer conditions at OWS P are shown in Fig. 4. The amplitudes of the anomalies (deviations from Gaussianity) are slightly smaller than the amplitudes of the observed anomalies (in particular for extended summer conditions). The basic structure, however, is captured by the simple linear inverse models: the multiplicative noise causes the distributions to have a more pronounced peak, weaker flanks, and heavier tails compared to a Gaussian distribution. That is, the multiplicative noise increases the kurtosis of the distribution. Thus, this simple model is able to explain the basic (neglecting the skew) non-Gaussian structure of the observed PDF (Fig. 1).

The effect of multiplicative noise in the linear stochastic models upon the spectrum of SST variability [Eq. (14)] at OWS P is shown in Fig. 5. Fig. 5a show two spectra for full-year conditions: the spectrum with pure additive is indicated by the dashed line, and the spectrum with multiplicative noise included is indicated by the solid line. Multiplicative noise enhances low-frequency SST variability of anomalous SST variability by about 20% (even as the total noise variance increases only by about 8%). The corresponding information for extended summer and winter (together with full-year) conditions is presented in Fig. 5b:

it shows the spectral densities ratios of the multiplicative noise models to the additive noise models. It can be seen that multiplicative noise generally enhances SST variability for all frequencies. The effect is strongest during winter, weakest during summer, and somewhere in between for all-year conditions.

4.2 Testing the multiplicative white-noise model

When we fit Eq. (11) to the data, we are making two assumptions: that the forcing is white, and that it is multiplicative. Neither, however, need be true to get a good linear fit of the autocorrelation function. These assumptions can be tested in a straightforward manner. The effective drift λ_{eff} estimated from data can be used to 'predict' T'_o after a time step Δt: $T'_o(t+\Delta t) = -\lambda_{eff}\, T'_{o\,Obs}(t)\,\Delta t + T'_{o\,Obs}(t)$. If the white-noise assumption is correct the difference between the observed value $T'_{o\,Obs}(t+\Delta t)$ and the predicted value $T'_o(t+\Delta t)$ should equal the white-noise forcing. The autocorrelation functions of the residuals $r \equiv T'_{o\,Obs}(t+\Delta t) - T'_o(t+\Delta t)$ for full-year, summer, and winter conditions are shown in Fig. 6a. The residuals are almost uncorrelated after one time step (one day), justifying the white-noise approximation.

The PDFs of the residuals (Fig. 6b) are very close to an exponential distribution (straight line in logarithmic plot) and are thus highly non-Gaussian. To test whether this residual represents multiplicative white-noise or merely non-Gaussian additive noise, we executed numerical experiments in which the model (10), with observed effective dampings λ_{eff} and additive noise whose distribution is the same as the residual, is integrated forward for 500000 days. The resulting PDFs differ from that in Figs. 1, 2, 4 and are nearly Gaussian.

This result is not entirely surprising, since a simple scaling argument also shows that non-Gaussian additive noise alone has no significant effect on the distribution of SST anomalies. Since $\lambda \sim [O(0.02)\,\mathrm{day}^{-1}]$ while $f'/h \sim [O(0.2)\,\mathrm{K\ day}^{-1}]$, $dT'_o/dt \approx f'/h$ so $T'_o \approx \sum_j f_j/h\,\Delta t$, and the Central Limit Theorem applies. In other words, for sufficiently small λ, non-Gaussian additive noise will result in a Gaussian distribution of SST anomalies T'_o. Thus, the non-Gaussianity of the observed PDF implies that the residual represents multiplicative noise.

4.3 A nonlinear stochastic inverse model

In the previous sections we showed that the linear model can explain the observed kurtosis of SST anomalies, but it cannot explain the observed skew. In this section we consider the most general (nondimensional) form of the univariate SDE that governs the evolution of SST anomalies,

$$\frac{dT'_o}{dt} = A(T'_o) + B(T'_o)\eta \quad , \tag{19}$$

where $A(T'_o)$ represents all slow processes and $B(T'_o)\eta$ represents the stochastic approximation to the fast nonlinear processes. The Gaussian white-noise η satisfies $\langle \eta(t) \rangle = 0$ and $\langle \eta(t)\eta(t') \rangle = \delta(t-t')$. Note that the deterministic dynamics in $A(T'_o)$ are no longer required to be linear and that $B(T'_o)\eta$ now represents both multiplicative and additive noise. As in the linear case, the multiplicative noise produces a drift, such that $A_{eff} = A + (1/2)\,B\,(\partial B/\partial T'_o)$ (e.g., Gardiner 2004).

Because the individual records from the OWSs are too short to accurately determine the nonlinear stochastic model of anomalous SST variability, we concatenated the normalized records from stations where stochastic theory is applicable, and where the skew has the same

sign: K in the North Atlantic, and P, N in the North Pacific (see the discussion in section 2). Note that the concatenated timeseries is nondimensional. As before, we analyzed full-year, extended winter, and extended summer conditions. However, in the concatenated record the differences between the full-year and the extended winter and summer seasons are minor, much less than those shown in section 4.1. For this reason we only present the full-year record in the remainder of this section.

The resulting PDF of the concatenated (full-year) record is shown in Fig. 7. As in the case of OWS P (Fig. 1), the PDF is calculated both as a normalized histogram (Fig. 7a) and as a MLE to a skew t-distribution (Fig. 7b). The PDF of the concatenated record has the same structure as the record from OWS P: it is clearly kurtosed and slightly skewed. Note, however, that the deviations from Gaussianity are larger for the concatenated record than for the OWS P record.

The nonlinear model can also be estimated from the data. The effective drift $A_{eff}(T'_o)$ is found by using its finite-difference definition

$$A_{eff}(T'_o) = \lim_{\Delta t \to 0} \frac{1}{\Delta t} \langle T'_o(t + \Delta t) - T'_o \rangle |_{T'_o(t)=T'_o} \tag{20}$$

(e.g., Siegert et al. 1998; Friedrich et al. 2000; Gradišek et al. 2000; Sura and Barsugli 2002; Sura 2003; Sura and Gille 2003); the result is shown in Fig. 8a (the error bars indicate $\pm$ one standard error). Note that $A_{eff}(T'_o)$ is almost linear and acts to damp anomalous SSTs. Therefore, a linear approximation is justified, as shown by the solid line: $A_{eff}(T'_o) \approx -0.023\, T'_o$. We next use the PDF $p(T'_o)$ and the effective drift $A_{eff}(T'_o)$ to determine $B(T'_o)$

from the Fokker-Planck equation (see Sura et al. 2005) corresponding to (19):

$$B(T_o') = \left(\frac{2}{p(T_o')} \int_{-\infty}^{T_o'} [A_{eff}(x')p(x')]\, dx' \right)^{1/2} . \tag{21}$$

The estimated noise $B(T_o')$ for the SST anomalies is shown by the solid line in Fig. 8b; the dotted line in Fig. 8b shows the optimal linear multiplicative noise obtained by fitting the variance and the kurtosis of the PDF (Fig. 7) to the linear SDE (11). The linear multiplicative noise qualitatively captures the main features of $B(T_o')$. However, there is clearly a nonlinear component to $B(T_o')$, since $B(T_o')$ is not symmetric with respect to $T_o' = 0$, and $B(T_o')$ increases more rapidly on the right hand side of the minimum at $T_o' \approx -0.8$ than on the left hand side (Fig. 8b). Therefore, the noise is stronger for positive SST anomalies than it is for negative anomalies, resulting in the observed skew. Note that the weak departure of $A(T_o')$ from linearity contributes very little to the observed skew and kurtosis.

We next use the effective drift $A_{eff}(T_o')$ and the noise $B(T_o')$ to determine the real deterministic drift $A(T_o')$. Shown in Fig. 9 are the noise-induced drift $(1/2)\, B\, (\partial B/\partial T_o')$, the real deterministic drift A, and the effective drift A_{eff}. Note that the noise-induced drift is almost linear and, as in the linear system discussed in the previous section, acts to undamp the system. That is, the results of the linear model are confirmed by the nonlinear model.

4.4 Predictability

We might expect that, due to the increase in persistence that results from the noise-induced drift, SST anomalies driven by multiplicative noise might be potentially more predictable than those driven by additive noise. The situation may, however, be complicated by increased

uncertainty resulting from the multiplicative noise itself. To assess this issue we compute a simple measure of predictability, the anomaly correlation of an ensemble mean perfect forecast with observations, which can be written as:

$$\rho_\infty(\tau) = \frac{S(\tau)}{\sqrt{S(\tau)^2 + 1}} \tag{22}$$

where $S(\tau) \equiv s(\tau)/\sigma(\tau)$ is the signal-to-noise ratio and τ is the forecast lead (e.g., Sardeshmukh et al. 2000; Newman et al. 2003b). Here the signal $s(\tau)$ is the ensemble mean, and the noise $\sigma(\tau)$ is the ensemble standard deviation. $\rho_\infty(\tau)$ is the expected skill of a perfect model in which the signal is determined as the mean of an infinite-member ensemble [see Sardeshmukh et al. (2000) or Newman et al. (2003b) for a more detailed discussion].

Two different stochastic models are compared the full multiplicative noise model (19), and a second "additive noise" model containing the same deterministic term $A(T'_o)$ but in which only additive noise, scaled to yield the (unit) variance of the concatenated SST anomaly timeseries, is used. That is, the variances of SST anomalies are the same in both the additive and the multiplicative noise models. Fig. 10 shows the forecast lead at which expected forecast skill ρ_∞ falls below 0.5, as a function of initial condition for the additive (dashed line) and the multiplicative noise model (solid line). In this simple example, multiplicative noise increases the lead time of skillful forecast from large negative SST anomalies (larger than one standard deviation) by about 5–10 days. Skill from positive anomalies is actually slightly worse, as in general skill from positive anomalies is lower than skill of similar amplitude negative anomalies. This result suggests that the anomalous heat flux derivative, parameterized as multiplicative noise, has a significant impact on the predictability of SST anomalies.

4.5 Spectra

Finally, the impact of multiplicative noise upon the low-frequency variability of SST anomalies is demonstrated by numerically integrating two different stochastic models, with and without multiplicative noise. Both models have the same deterministic dynamics $A(T'_o)$, but the additive noise model uses pure additive noise (the strength of the additive noise is given by the minimum of $B(T'_o)$), whereas the multiplicative noise model uses the full multiplicative noise term $B(T'_o)$ (Fig. 8b). The spectra of both models are shown in Fig. 11. The spectrum with pure additive noise is indicated by the dashed line, and the spectrum with multiplicative noise included is indicated by the solid line.

Multiplicative noise enhances the low-frequency variability of anomalous SST variability by about 100% (even as the total noise variance increases only by about 30%). The linear model for OWS P showed that the multiplicative noise enhanced the low-frequency variability of anomalous SST variability by about 20%, whereas the total noise variance increased by about 8% (Fig. 5). Why is there such a difference between OWS P and the concatenated record? The non-Gaussianity of the concatenated SST anomaly record is larger than the non-Gaussianity at OWS P, resulting in correspondingly stronger multiplicative noise. As confirmed by a linearization of $A(T'_o)$ and $B(T'_o)$, the spectral difference between OWS P and the concatenated record is mainly due to the different strengths of the multiplicative noises and not to nonlinear effects. That means, the linear approximations of $A(T'_o)$ and $B(T'_o)$ are very good representations (neglecting the skew) of the underlying physical processes. Again, the results of the linear model are confirmed by the nonlinear model.

5 Mixed Layer Ocean Model

In section 3 we used a simple conceptual model, along the lines of the original FH study, to propose that the non-Gaussianity of observed SST variability is the consequence of multiplicative noise in the surface heat flux. As a test of this hypothesis, we showed that daily SST observations at several OWS are consistent with a multiplicative noise model; in particular, the observed non-Gaussianity is primarily the result of rapidly decorrelating nonlinearity (i.e., multiplicative noise), whereas the deterministic term ($A(T'_o)$; i.e., the slowly evolving dynamics) is effectively linear. Of course, the drawback of inverse stochastic modeling is that while it can clarify the dynamical form of a system, it does not always clarify which physical processes are dominant. Also, the form of $B(T'_o)$ is not linear (as our simple conceptual model had suggested), and other terms in the mixed layer heat budget, such as horizontal advection, entrainment, and mixed-layer depth variability, might also contribute to the non-Gaussianity. In addition, the effects of pronounced seasonality both in the mixed layer depth and the atmospheric noise may have been obscured by the extended seasons we have defined.

Therefore, to diagnose the physical processes responsible for $B(T'_o)$ and to test some of our assumptions, we next carry out a simple modeling study. We will use a single column variable-depth mixed layer model to attempt to reproduce the observed PDFs at OWS P, determine whether this non-Gaussianity can again be modeled stochastically, and determine if all terms in the mixed layer heat budget can be reasonably approximated by multiplicative noise. This model clearly does not have advection terms (either in the ocean or atmosphere), and does not include air-sea coupling, so their relative importance will be assessed by their

absence.

5.1 Model description

The single column mixed layer model we use was developed by Gaspar (1988) and later used by Alexander and Penland (1996) and Alexander et al. (2000), among many others. The tendency of the mixed layer temperature T_o is given by

$$\frac{\partial T_o}{\partial t} = \frac{Q_{net} - Q_{swh}}{\rho_w \, C_h \, h} + \frac{W_e \Delta T}{h} + CA - \frac{\kappa}{h} \frac{\partial T}{\partial z}\Big|_{z=h} \tag{23}$$

where $\Delta T = T_b - T_o$ (T_b is the temperature just below the mixed layer), Q_{net} is the net surface energy flux into the ocean, Q_{swh} is the penetrating solar radiation at the mixed layer depth $z = h$, W_e is the entrainment rate, ρ_w and C_h are the reference density and specific heat of sea water, κ is the vertical mixing coefficient, and z the vertical coordinate. Convective adjustment (CA) occurs when the mixed layer is more dense than the layer below. Salinity is set to climatology, since long time series of precipitation over the oceans, which strongly influences salinity, are unavailable. The region beneath the mixed layer is represented by a multi-layer system, where heat is redistributed through convective overturning, vertical diffusion, and penetrating solar radiation. The model contains 30 unequally spaced layers between the surface and 1000 m, where 15 layers are within the first 100 m in order to adequately resolve the summer thermocline. A more detailed description of the model can be found in Alexander et al. (2000).

The seasonally varying atmospheric forcing, based on 30 years of data from OWS P, consists of three independent Markov models for anomalous air temperature, wind speed,

and solar radiation, while the dewpoint temperature anomaly mainly depends on the air temperature anomaly. Note that these parameters are simulated as slightly red noise with a decorrelation time scale of about 3 days. In addition, a second lower amplitude slower red-noise (with a time scale of 28 days) is added to the temperature to simulate observed slower variability associated with external forcing and/or air-sea coupling; there is no actual air-sea coupling in this model. The anomalies are then added to the mean seasonal cycle of their respective fields and used to compute the forcing fields for the mixed layer model. The atmosphere and the ocean are integrated using a 1-hour time step in order to obtain reasonable statistics for the atmospheric variables. The ocean is forced by the atmosphere every time step. Further on we will use daily averaged ocean quantities to compare with the daily averaged observations. The mixed layer model realistically simulates both the mean and standard deviation of ocean temperature over the seasonal cycle. See Alexander and Penland (1996) for details of the forcing and the modeled mean climatology at OWS P.

5.2 Results

5.2.1 PDFs and stochasticity

The model is run for 5000 yrs, which allows accurate determination of PDFs of daily SST anomalies for each calendar month. Deviations from Gaussianity of the PDFs of daily data grouped by each month, and also by extended winter (November-April) and extended summer (May-October) seasons, are shown in Fig. 12. Comparison with the observed PDFs (Fig. 2) shows that the mixed layer model simulates the non-Gaussianity of SST anomalies

well throughout the months of November-April. However, modeled non-Gaussianity in the months of May-October is generally weaker than is observed. This result does not appear to be due to the relatively larger sample of model output, since subsampling the model run yields similar results. The poorer summertime simulation could be due to an artificial constraint on the mixed layer, which must always exist as a single layer and is not allowed to be shallower than 10 m. Missing physics that may be particularly important during summer, such as feedback between anomalous SST and clouds (e.g., Norris and Leovy 1994; Klein et al. 1995; Norris 2000), could also contribute to biases found in the mixed layer model. Therefore, we will focus upon the physical processes that drive non-Gaussianity during extended winter.

The stochastic model [the effective drift $A_{eff}(T'_o)$ and noise $B(T'_o)$; see Eq. (19)] of extended winter SST anomalies from the mixed layer model, shown in Fig. 13, is generally similar to the stochastic model constructed from observations (Fig. 8). The effective drift of the simulated SST anomalies (Fig. 13a) is almost linear. As was the case for the observed drift, the small departures from linearity of $A_{eff}(T'_o)$ cannot explain the non-Gaussianity of the PDFs. Likewise, the noise (Fig. 13b) of the modeled SST anomalies shows the same general state-dependent structure earlier found for observations, with the notable exception that the minimum of $B(T'_o)$ is nearer to $T'_o = 0$ than $T'_o = -1$. Also shown in Fig. 13 are the stochastic models determined separately for each month. The relatively minor month-to-month variations of both the PDFs (Fig. 12) and stochastic terms justifies the use of the extended winter in the observational analysis and suggests that observed non-Gaussianity during the extended winter is not a result of seasonal variation of mean quantities and/or

atmospheric noise forcing.

5.2.2 SST tendency budget

Since the mixed layer model reproduces the PDFs and the stochastic dynamics of the wintertime observations reasonably well, the SST tendency budget can be used to assess how different physical processes contribute to the non-Gaussianity (i.e., skewness and kurtosis) of anomalous SST variability. Following Alexander and Penland (1996) variables are split into a daily mean ($\langle\,\rangle$) and a deviation from the mean ($'$). Assuming that the mixed layer depth anomaly h' is much smaller than the mean $\langle h\rangle$, a valid approximation for wintertime conditions at OWS P, the anomalous mixed layer temperature tendency can be approximated by

$$\frac{\partial T_o'}{\partial t} \approx \frac{Q_{net}'}{\rho_w\, C_h\, \langle h\rangle} - \frac{\langle Q_{net}\rangle h'}{\rho_w\, C_h\, \langle h\rangle^2} - \left(\frac{Q_{net}' h'}{\rho_w\, C_h\, \langle h\rangle^2} - \frac{\langle Q_{net}' h'\rangle}{\rho_w\, C_h\, \langle h\rangle^2}\right) + \mathcal{E} \tag{24}$$

where $\mathcal{E}$ denotes all entrainment, overturning, and mixing effects. During the winter, the anomalous mixed layer temperature (SST) tendency is predominantly due to net heat flux anomalies, that is, the first term on the right hand side of (24) (Alexander and Penland 1996). Therefore, we can approximate (24) as

$$\frac{\partial T_o'}{\partial t} \approx \frac{Q_{net}'}{\rho_w\, C_h\, \langle h\rangle} \equiv f' \tag{25}$$

where f' is the anomalous net heat flux.

The multiplicative noise characteristics of the anomalous net heat flux is clearly seen by plotting f' as a function of the air-sea temperature anomaly difference, as shown in Fig. 14a. While f' can be well fitted by a linear function with slope β [$\beta(T_a' - T_o')$; see line in Fig. 14a],

the instantaneous f' values have a scatter around this line whose amplitude is not constant but instead depends upon $(T'_a - T'_o)$. That is, we can write (25) as:

$$\frac{\partial T'_o}{\partial t} = \beta(T'_a - T'_o) + \eta[(T'_a - T'_o)] \tag{26}$$

where the amplitude of the residual η is a function of $T'_a - T'_o$. The tests used earlier in section 4.2 are again applied to demonstrate that η acts as multiplicative white noise. Interestingly, the white noise approximation is somewhat better for observations than for the model output, since η decorrelates on a time scale of about 3-5 days (cf. Fig. 6a), still far shorter than the 60-70 day timescale implicit in β. The redder residual may be due to the (uncoupled) model atmosphere being somewhat too red; see, for example, Fig. 1 of Alexander and Penland (1996).

If we approximate $\eta[(T'_a - T'_o)] = (T'_a - T'_o)\eta_o$, where η_o is Gaussian white noise, then (26) becomes

$$\frac{\partial T'_o}{\partial t} = (\beta + \eta_o)(T'_a - T'_o) \tag{27}$$

or

$$\frac{\partial T'_o}{\partial t} = -\beta T'_o - \eta_o T'_o + (\beta T'_a + \eta_o T'_a) \tag{28}$$

That is, the net heat flux anomaly has the same form as in our simple model (see section 3). Note that in the context of this model, where T'_a is an external variable, both atmospheric forcing terms $\beta T'_a$ and $\eta_o T'_a$ are "fast", or stochastic, forcings because T'_a rapidly varies with a decorrelation time scale of about 3 days. Although the latter term is highly non-Gaussian, it represents additive noise and thus has only minimal impact on the distribution of SST

anomalies because of the Central Limit Theorem (see section 4.2). The state-dependent noise term is linear multiplicative noise, as in our simple model [Eq. 11 and Fig. 8b]. However, it is obvious from the scatter in Fig. 14a, as well as the earlier observational study, that although approximating η as a linear multiplicative noise term captures much of its behavior, it is better modeled as a non-linear state-dependent noise. Note also that the scatter in Fig. 14a, which represents the multiplicative noise [cf. Eq. (27)], matches the term $B(T'_o)$ in Fig. 8b, which includes both additive noise and multiplicative noise [cf. Eq. (28)]. Thus, as $B(T'_o)$ has generally larger amplitude for positive SST anomaly, the scatter in Fig. 14a is greater for negative $T'_a - T'_o$.

Finally, we determine how the individual component fluxes (sensible and latent heat fluxes, and short and long wave radiation fluxes, shown in Fig. 14b-e) contribute to the multiplicative nature of the total heat flux. The scatter of anomalous sensible heat flux anomalies (Fig. 14b) most clearly demonstrates nearly linear multiplicative noise, with the amplitude of the noise dropping to almost zero for $T_a - T_o = 0$ (that is, $T'_a - T'_o \approx 0.7$). For the latent heat flux (Fig. 14c), there is a similar minimum at $T_d - T_o = 0$ (that is, $T'_a - T'_o \approx 3$), where T_d is the dewpoint temperature. This minimum is shifted since $\langle T_d \rangle < \langle T_a \rangle$. Also, since T_d is not perfectly correlated with T_a, the scatter is never zero.

Note that the sensible heat flux actually represents almost piecewise linear multiplicative noise; that is, linear multiplicative noise where the amplitude is different for positive and negative values of $T_a - T_o$. This results from the bulk transfer coefficient having a larger (constant) amplitude for unstable ($T_a - T_o < 0$) than stable ($T_a - T_o > 0$) conditions (Large and Pond 1982). A similar effect exists for the latent heat flux. A second model run in which

the stability dependence of the transfer coefficient is removed has its skewness reduced by about 40%.

Some of the remaining skew results from the anomalous latent heat flux due to the nonlinearity inherent to the Clausius-Clapeyron equation. For warmer SST (decreasing $T'_a - T'_o$), relatively larger specific humidity anomalies give rise to larger amplitude latent heat flux noise. Because of the exponential nature of the Clausius-Clapeyron relationship, this suggests that (all other things being equal) regions with warmer SST could have increased skewness.

Most of the remaining skew, however, is a consequence of mean state differences between the ocean and atmosphere that results in noise terms like $|\mathbf{U}|'(\langle T_a \rangle - \langle T_o \rangle)$ and $|\mathbf{U}|'(\langle q_a \rangle - \langle q_s \rangle)$ within the anomalous surface heat flux. If the mean state differences were zero, these terms would be zero and for constant transfer coefficients the scatter of the fluxes would be symmetric around $T'_a - T'_o = 0$. Since these noise terms are not zero, they introduce the asymmetry (noted above) that results in skew. Recall that this effect is more pronounced in Fig. 14c since the latent heat flux is related to the dewpoint temperature T_d and not the atmospheric temperature T_a. This asymmetry is essentially a manifestation of correlated noise; that is, portions of the additive and multiplicative noises are correlated because they both depend upon the atmospheric noise $|\mathbf{U}|'$.

Strictly speaking, the slow dynamics represented by $A(T'_o)$ also include the nonlinearity in both the bulk transfer coefficients and Clausius-Clapeyron equation. However, as noted above, this small deviation is not responsible for the modeled non-Gaussianity.

The anomalous radiative terms are shown in Fig. 14d (short-wave) and Fig. 14e (long-wave). Note that scatter of the anomalous long-wave heat flux is so small that it is masked by the linear fit. Moreover, in this model there is no state-dependence for the short-wave fluxes. Clearly, there are negligible radiative effects in the multiplicative noise $B(T'_o)$. In conclusion, this model suggests that during extended winter anomalous SST variability at OWS P is non-Gaussian largely as a result of multiplicative noise present in the sensible and latent heat fluxes.

6 Summary and Discussion

In this paper we showed that distributions of daily SST anomalies at several Ocean Weather Stations are non-Gaussian. Broadly speaking, the distributions have a stronger peak, weaker flanks, and heavier tails than the related Gaussian distributions. With the exception of OWS V, all have positive skew. We suggested that this observed non-Gaussianity can be understood with a simple extension to the FH stochastic model of midlatitude SST anomalies, accounting for the effect of rapid variability of surface winds (parameterized as noise) upon both the surface heat flux and the surface heat flux derivative (with respect to SST). The latter effect results in multiplicative noise and has been ignored in many simple stochastic models (e.g., Frankignoul and Hasselmann 1977).

Our key point is that inclusion of this multiplicative noise term allows the FH model to qualitatively reproduce not only an exponential autocorrelation function, but also the main features of the observed distributions of SST anomalies. The model (counterintuitively)

also predicts that this multiplicative noise can increase the persistence, predictability, and low-frequency variability of midlatitude SST anomalies. That is, part of the observed autocorrelation of SST anomalies is due to the noise-induced drift.

Details of the non-Gaussianity, and particularly the skew, do not require the deterministic (slow dynamics) term $A(T'_o)$ to be nonlinear but do require the multiplicative noise term $B(T'_o)$ to depart from linearity, as was found in both the inverse stochastic model and the single column model. Our results suggest that even then much of this skew may be understood by allowing $B(T'_o)$ to be piecewise linear and to include a correlated noise component. An important underlying physical cause in both cases is the dependence of the noise on boundary layer stability, since correlated noise depends upon mean stability and since the bulk transfer coefficient is smaller for stable conditions (colder SST) than unstable conditions (warmer SST). Increased positive skew, such as at OWS N, might then result from warmer SST giving rise to increased low-level instability. Regions where latent heat flux is relatively strong compared to the sensible heat flux, both due to warmer SST and/or drier air, should also have greater positive skew because of both nonlinearity of the Clausius-Clapeyron equation and enhanced correlated noise. OWS V, however, displays negative skew, suggesting that our model is incomplete. An obvious possibility is that ocean dynamics are more important at this station (which is near the edge of the North Pacific current); another possibility is that complex atmospheric dynamics and coupling between ocean and atmosphere in this region cannot be ignored as in our simple model.

Earlier studie considering multiplicative noise forcing of SST (e.g., Neelin and Weng 1999) suggested that changes in the SST anomaly could produce changes in atmospheric variability

and thus in the forcing term f'. Note that in our study, multiplicative noise forcing of the mixed layer exists even if the atmosphere is *not* sensitive to changes in midlatitude SST. Still, if atmospheric noise in (11) is a function of T'_o, for example if $\sqrt{2M}\,T'_o$ is replaced with $\sqrt{2M(T'_o)}\,T'_o$, then the multiplicative noise might no longer be linear. For example, recent observational studies suggest state-dependence of boundary-layer fluxes due to positive local (on scales smaller than 1000 km) correlation between SSTs and sea surface winds (Chelton et al. 2004; O'Neill et al. 2003; Small et al. 2005; Xie 2004), perhaps because decreased stability in the atmospheric boundary layer over warm (cold) SSTs increases (decreases) the wind stress through enhanced (reduced) downward turbulent mixing of momentum. This is another possible source of the small deviation of $B(T'_o)$ from linearity seen in Fig. 8b. Clearly, though, any significant dependence of atmospheric noise upon the SST anomaly implies the need for a stochastic coupled model, such as that employed by Barsugli and Battisti (1998). They suggested that coupling enhances the thermal variance in the ocean and the atmosphere by reducing the anomalous air-sea temperature difference. How surface wind variability impacts their model is a focus of our current research; note that they considered only thermal noise, whereas changes in wind variability due to the SST anomaly may require non-local feedbacks and consideration of boundary layer stability.

We have also not considered forcing of midlatitude oceans, particularly the North Pacific, by the atmospheric bridge that results from ENSO (e.g., Alexander et al. 2002; Newman et al. 2003a). Noise-induced drift could enhance the mean response to ENSO forcing (Sardeshmukh et al. 2001), particularly where ENSO also increases high-frequency atmospheric variability (Smith and Sardeshmukh 2000; Compo et al. 2001). For multivariate systems, external

forcing can result in a skewed PDF even if the multiplicative noise term is linear (Sura et al. 2005).

Our results demonstrate that the high-frequency variability of boundary-layer winds and related heat fluxes are crucial for understanding low-frequency anomalous SST variability. That is, we see a scale interaction between the fast wind induced heat flux variability and the slow SST variability. This scale interaction has implications for atmospheric forcing employed in ocean models, suggesting that the high-frequency variability of boundary layer winds and related surface fluxes must be accurately simulated to correctly model low-frequency variability of SSTs. That is, a coupled model with incorrect atmospheric variability (i.e., noise) might incorrectly estimate SST variability and related atmosphere-ocean coupling. For example, many atmospheric models (but not all) significantly underestimate wind variability in the marine boundary layer (e.g., Gille 2005; Monahan 2005b,a). It is unclear how a bias in wind variability (and related heat fluxes) contributes to biases found in many coupled models. However, we have a powerful theory/tool at hand to systematically study this problem. The results could guide the development of improved coupling schemes and the implementation of stochastic parameterizations in climate models.

Acknowledgments. The authors wish to thank Drs. Adam Monahan and Birol Kara and one anonymous reviewer whose comments greatly improved this paper. This work was partially supported by a grant from NOAA CLIVAR/Pacific.

References

Alexander, M. A., I. Blade, M. Newman, J. R. Lanzante, N.-C. Lau, and J. D. Scott, 2002: The atmospheric bridge: The influence of ENSO teleconnections on air-sea interaction over the global ocean, *J. Climate*, **14**, 2205–2231.

Alexander, M. A., and C. Penland, 1996: Variability in a mixed layer ocean model driven by stochastic atmospheric forcing, *J. Climate*, **9**, 2424–2442.

Alexander, M. A., and J. D. Scott, 1997: Surface flux variability over the North Pacific and North Atlantic oceans, *J. Climate*, **10**, 2963–2978.

Alexander, M. A., J. D. Scott, and C. Deser, 2000: Processes that influence sea surface temperature and ocean mixed layer depth variability in a coupled model, *J. Geophys. Res. Oceans*, **105**, 16823–16842.

Anteneodo, C., and C. Tsallis, 2003: Multiplicative noise: A mechanism leading to nonextensive statistical mechanics, *J. Math. Phys.*, **44**, 5194–5203.

Azzalini, A., and A. Capitanio, 2003: Distributions generated by perturbations of symmetry with emphasis on a multivariate skew *t*-distribution, *J. R. Statist. Soc. B*, **65**, 367–389.

Barsugli, J. J., and D. S. Battisti, 1998: The basic effects of atmosphere-ocean thermal coupling on midlatitude variability, *J. Atmos. Sci.*, **55**, 477–493.

Blaauboer, D., G. J. Komen, and J. Reiff, 1982: The behaviour of the sea surface temperature (SST) as a response to stochastic latent- and sensible heat forcing, *Tellus*, **34**, 17–28.

Chelton, D. B., M. G. Schlax, M. H. Freilich, and R. F. Milliff, 2004: Satellite measurements reveal persistent small-scale features in ocean winds, *Science*, **303**, 978–983.

Compo, G. P., P. D. Sardeshmukh, and C. Penland, 2001: Changes of subseasonal variability associated with El Niño, *J. Climate*, **14**, 3356–3374.

Diaz, H. F., C. S. Ramage, S. D. Woodruff, and T. S. Parker, 1987: *Climatic Summaries of Ocean Weather Ships*, Tech. rep., U.S. Department of Commerce (NOAA) and University of Colorado (CIRES).

Dinsmore, R. P., 1996: Alpha, Bravo, Charlie... Ocean Weather Ships 1940-1980, *Oceanus*, **39**, 9–10.

Frankignoul, C., and K. Hasselmann, 1977: Stochastic climate models. Part II. Application to sea-surface temperature anomalies and thermocline variability, *Tellus*, **29**, 289–305.

Friedrich, R., S. Siegert, J. Peinke, S. Lück, M. Siefert, M. Lindemann, J. Raethjen, G. Deusch, and G. Pfister, 2000: Extracting model equations from experimental data, *Phys. Lett. A*, **271**, 217–222.

Gardiner, C. W., 2004: *Handbook of Stochastic Methods for Physics, Chemistry and the Natural Science, Third Edition*, Springer-Verlag, 415 pp.

Gaspar, P., 1988: Modeling the seasonal cycle of the upper ocean, *J. Phys. Oceanogr.*, **18**, 161–180.

Gille, S. T., 2005: Statistical characterization of zonal and meridonal ocean wind stress, *J. Atmos. Ocean. Tech.*, in press.

Gradišek, J., S. Siegert, R. Friedrich, and I. Grabec, 2000: Analysis of time series from stochastic processes, *Phys. Rev. E*, **62**, 3146–3155.

Hall, A., and S. Manabe, 1997: Can local linear stochastic theory explain sea surface temperature and salinity variability?, *Climate Dyn.*, **13**, 167–180.

Hasselmann, K., 1976: Stochastic climate models. Part I. Theory, *Tellus*, **28**, 473–484.

Jones, M. C., and M. J. Faddy, 2003: A skew extension of the *t*-distribution, with applications, *J. R. Statist. Soc. B*, **65**, 159–174.

Klein, S. A., D. L. Hartmann, and J. R. Norris, 1995: On the relationships among low-cloud structure, sea surface temperature and atmospheric circulation in the summertime northeast Pacific, *J. Climate*, **8**, 1140–1155.

Kloeden, P., and E. Platen, 1992: *Numerical Solution of Stochastic Differential Equations*, Springer-Verlag, 632 pp.

Large, W. G., and S. Pond, 1982: Sensible and latent heat flux measurements over the oceans, *J. Phys. Oceanogr.*, **12**, 464–482.

Monahan, A. H., 2005a: The probability distributions of sea surface wind speeds Part I: Dataset intercomparison and seasonal variability, *J. Climate*, in press.

Monahan, A. H., 2005b: The probability distributions of sea surface wind speeds Part I: Theory and SSM/I observations, *J. Climate*, in press.

Neelin, J. D., and W. Weng, 1999: Analytical prototypes for ocean-atmosphere interaction

at midlatitudes. Part I: Coupled feedbacks as a sea surface dependent stochastic process, *J. Climate*, **12**, 2037–2049.

Newman, M., G. P. Compo, and M. A. Alexander, 2003a: ENSO-forced variability of the Pacific Decadal Oscillation, *J. Climate*, **16**, 3853–3857.

Newman, M., P. D. Sardeshmukh, C. R. Winkler, and J. S. Whitaker, 2003b: A study of subseasonal variability, *Mon. Wea. Rev.*, **31**, 1715–1732.

Norris, J. R., 2000: Interannual and interdecadal variability in the storm track, cloudiness, and sea surface temperature over the summertime North Pacific, *J. Climate*, **13**, 422–430.

Norris, J. R., and C. Leovy, 1994: Interannual variability in stratiform cloudiness and sea surface temperature, *J. Climate*, **7**, 1915–1925.

O'Neill, L. W., D. B. Chelton, and E. S K, 2003: Observations of sst-induced perturbations of the wind stress field of the Southern Ocean on seasonal time scales, *J. Climate*, **16**, 2340–2354.

Paul, W., and J. Baschnagel, 1999: *Stochastic Processes: From Physics to Finance*, Springer-Verlag, 231 pp.

Peinke, J., F. Böttcher, and S. Barth, 2004: Anomalous statistics in turbulence, financial markets and other complex systems, *Ann. Phys.*, **13**, 450–460.

Penland, C., 2003a: Noise out of chaos and why it won't go away, *Bulletin of the American Meteorological Society*, **84**, 921–925.

Penland, C., 2003b: A stochastic approach to nonlinear dynamics: A review (electonic supplement to 'noise out of chaos and why it won't go away'), *Bulletin of the American Meteorological Society*, **84**, ES43–ES51.

Reynolds, R., 1978: Sea surface temperature anomalies in the North Pacific Ocean, *Tellus*, **30**, 97–103.

Ronca, R. E., and D. S. Battisti, 1997: Anomalous sea surface temperatures and local air-sea energy exchange on intraannual timescale in the northeastern subtropical Pacific, *J. Climate*, **10**, 102–117.

Sakaguchi, H., 2001: Fluctuation dissipation relation for a Langevin model with multiplicative noise, *J. Phys. Soc. Jpn.*, **70**, 3247–3250.

Sardeshmukh, P., C. Penland, and M. Newman, 2001: Rossby waves in a fluctuating medium, *Progress in Probability, Vol. 49: Stochastic Climate Models*, P. Imkeller, and J.-S. von Storch, eds., Birkhäuser Verlag, Basel.

Sardeshmukh, P. D., G. P. Compo, and C. Penland, 2000: Changes of probability associated with El Niño, *J. Climate*, **13**, 4268–4286.

Siegert, S., R. Friedrich, and J. Peinke, 1998: Analysis of data sets of stochastic systems, *Phys. Lett. A*, **243**, 275–280.

Small, R. J., S.-P. Xie, and J. Hafner, 2005: Satellite observations of mesoscale ocean features and copropagating atmospheric surface fields in the tropical belt, *J. Geophys. Res.*, **110**, C02021.

Smith, C. A., and P. D. Sardeshmukh, 2000: The effect of ENSO on the intraseasonal variance of surface temperatures in winter, *Int. J. Climatol.*, **20**, 1543–1557.

Sura, P., 2003: Stochastic analysis of Southern and Pacific Ocean sea surface winds, *J. Atmos. Sci.*, **60**, 654–666.

Sura, P., and J. J. Barsugli, 2002: A note on estimating drift and diffusion parameters from timeseries, *Phys. Lett. A*, **305**, 304–311.

Sura, P., and S. T. Gille, 2003: Interpreting wind-driven Southern Ocean variability in a stochastic framework, *J. Mar. Res.*, **61**, 313–334.

Sura, P., M. Newman, C. Penland, and P. D. Sardeshmukh, 2005: Multiplicative noise and non-Gaussianity: A paradigm for atmospheric regimes?, *J. Atmos. Sci.*, **62**, 1391–1409.

Xie, S.-P., 2004: Satellite observations of cool ocean-atmosphere interaction, *Bulletin of the American Meteorological Society*, **85**, 195–208.

Table 1: The Ocean Weather Stations (OWSs) used for this study.

OWS	Location	Period
P	50°N, 145° W	1949–1981
N	30°N, 140° W	1946–1974
V	34°N, 164° E	1955–1971
K	45°N, 16° W	1949–1975

Table 2: Parameters used to scale the heat flux equations for typical conditions at Ocean Weather Station P.

Air density	$\rho_A = 1.225$ Kg m^{-3}
Sea-water density	$\rho_W = 1024$ Kg m^{-3}
Mixed layer depth	$h = 50$ m
Inverse Bowen ratio	$B = 8$
Bulk transfer coefficient	$C_H = 1.5 \times 10^{-3}$
Specific heat of air	$C_a = 1004$ J Kg^{-1} K^{-1}
Specific heat of sea-water	$C_h = 4187$ J Kg^{-1} K^{-1}
Mean wind speed	$\langle \lvert\mathbf{U}\rvert \rangle = 8$ m s^{-1}
Anomalous wind speed (rms)	$\lvert\mathbf{U}\rvert' = 4$ m s^{-1}

Table 3: Parameters of linear inverse models for OWS P .

Parameter	full-year	extended summer	extended winter
λ_{eff} [day^{-1}]	0.0157 ± 0.0002	0.024 ± 0.0004	0.0167 ± 0.0003
$\sqrt{2M}$ [day$^{-1/2}$]	0.047 ± 0.006	0.045 ± 0.007	0.060 ± 0.008
$\sqrt{2D}$ [K day$^{-1/2}$]	0.144 ± 0.001	0.195 ± 0.003	0.117 ± 0.002

a)

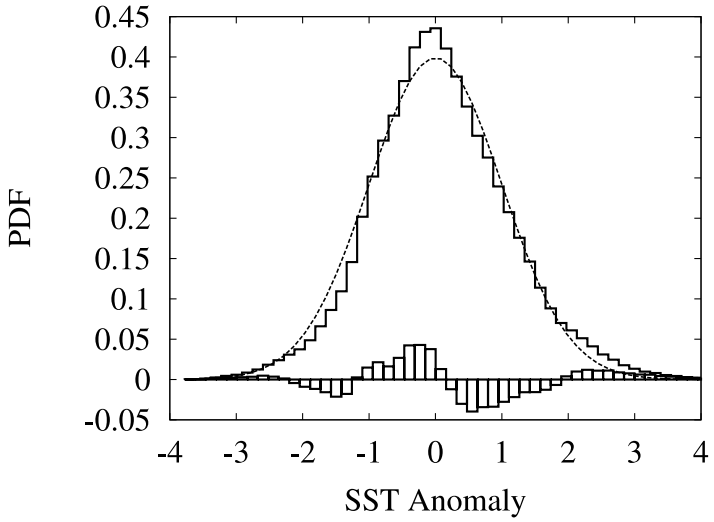

b)

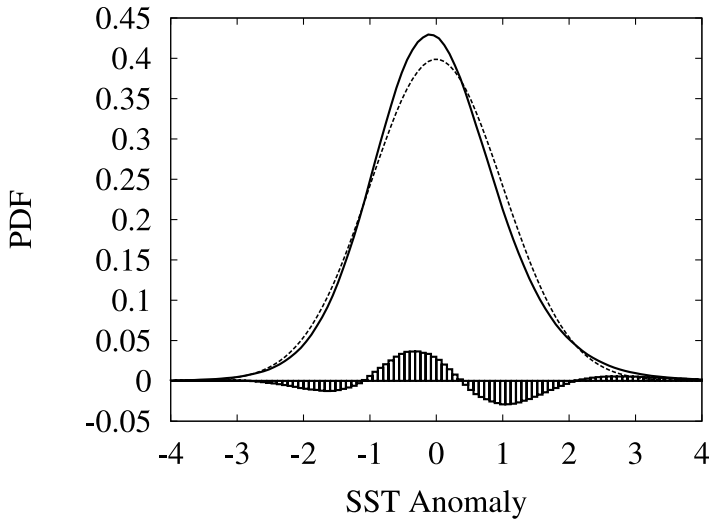

Figure 1: The PDFs of SST anomalies (in K) at OWS P, related Gaussian distributions, and deviations from Gaussianity. In (a) the PDF (steps) is calculated as a normalized histogram. The dashed line is the related Gaussian distribution, whereas the boxes denote deviations from Gaussianity. Note that the PDF has a strong peak, weak flanks, and heavy tails relative to a Gaussian distribution (the PDF is kurtosed). Furthermore, the PDF is slightly skewed. In (b) the PDF (solid line) is calculated as a MLE to a skew t-distribution. The dashed line is the related Gaussian distribution, whereas the boxes denote deviations from Gaussianity.

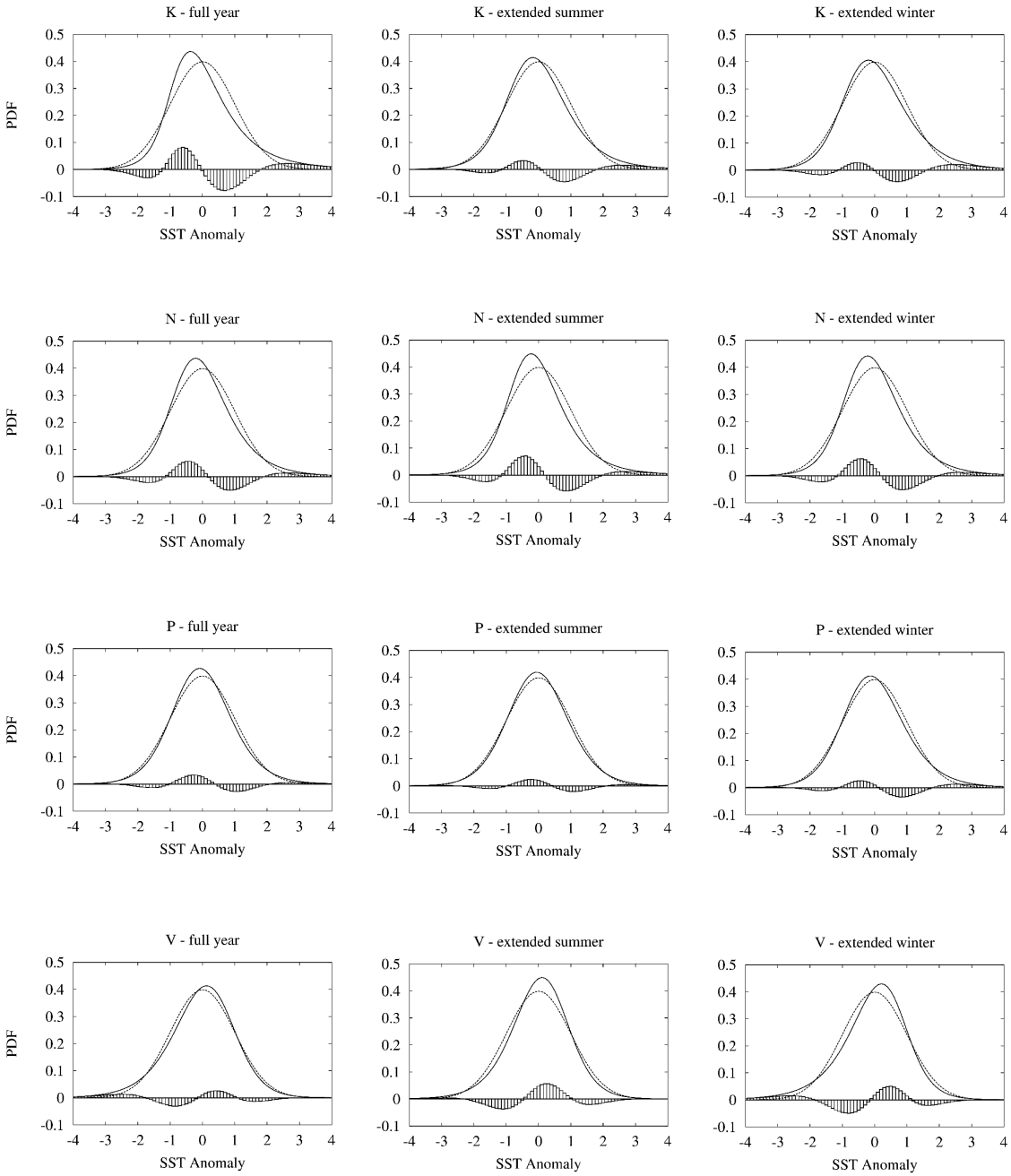

Figure 2: The PDFs of SST anomalies (normalized to make comparison possible) at locations where stochastic theory is applicable: P, N , and V in the North Pacific, and K in the North Atlantic (see Table 1 for the locations and recording periods). The PDFs (solid line) are calculated as a MLE to a skew t-distribution. The dashed lines are the related Gaussian distributions, whereas the boxes denote deviations from Gaussianity.

a)

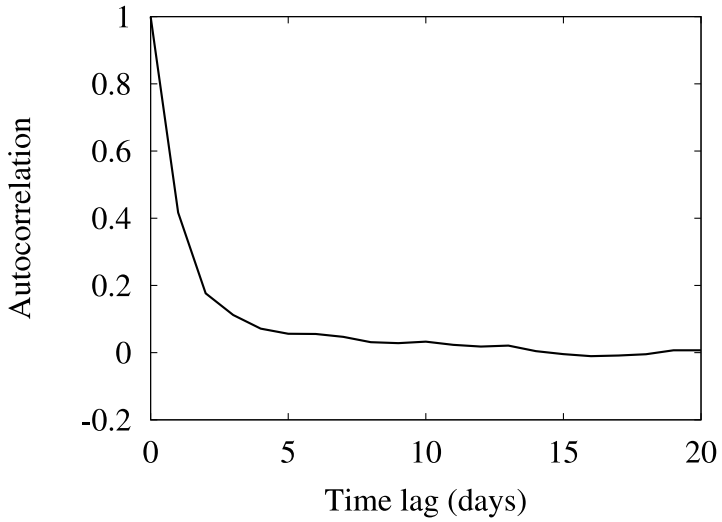

b)

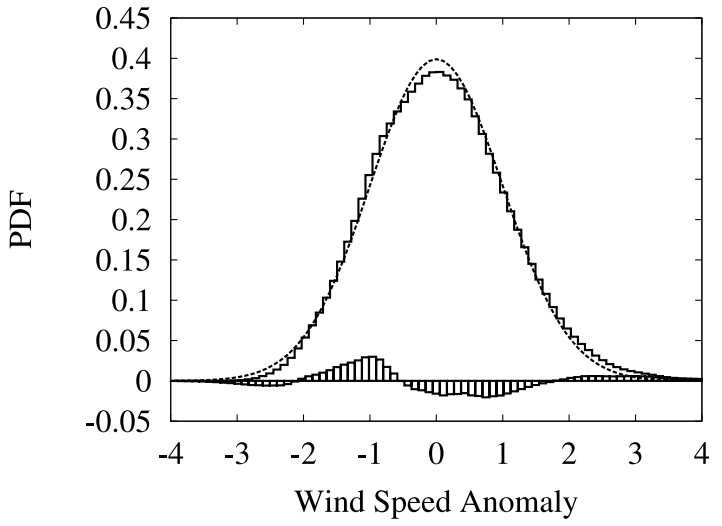

Figure 3: (a) Autocorrelation function and (b) PDF of wind speed anomalies (m/s) at OWS P.

a) full-year

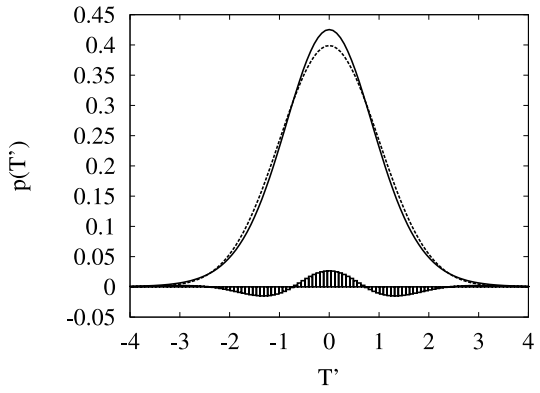

b) summer

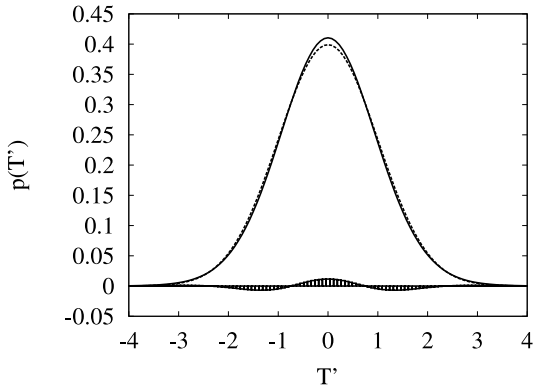

c) winter

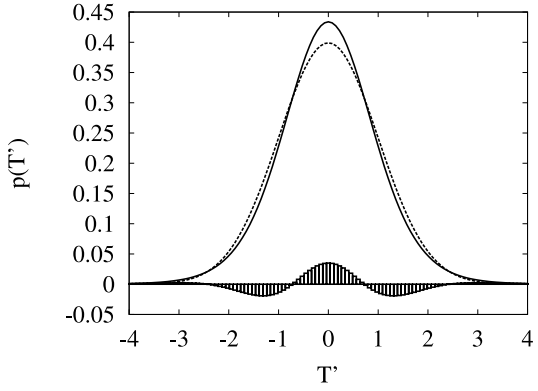

Figure 4: Stationary SST anomaly (in K) probability distributions $p(T'_o)$ [in the figure $p(T'_o) \equiv p(T')$] for OWS P given by Eqs. (15) and (16) for (a) full-year, (b) extended summer, and (c) extended winter conditions (together with the related Gaussian distributions and deviations from Gaussianity as in Figs. 1 and 2). Note that the general structure of the analytically derived PDFs is close to that of the observed ones (Figs. 1 and 2).

a) full-year

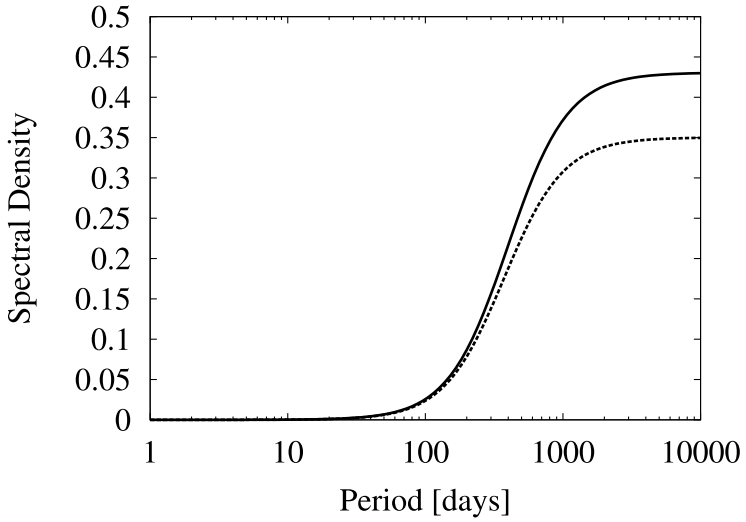

b)

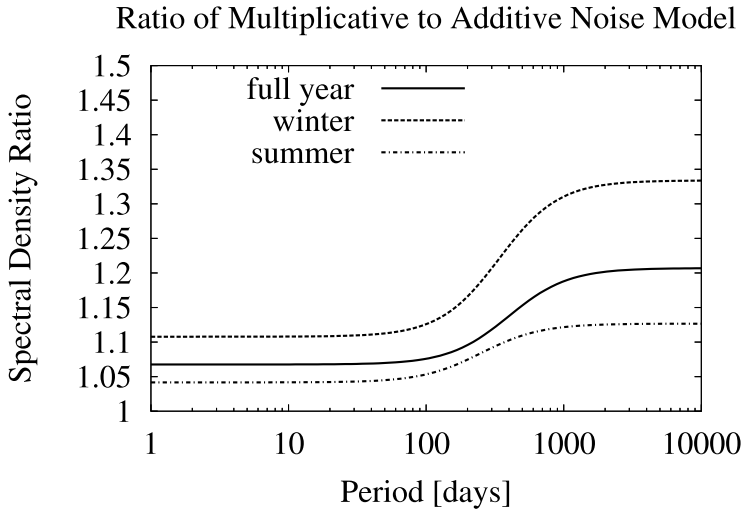

Figure 5: (a) Spectra of linearly modeled anomalous SST variability without and with muliplicative noise given by Eq. (14) for OWS P full-year conditions. The spectrum with pure additive noise is indicated by the dashed line, and the spectrum with multiplicative noise included is indicated by the solid line. It can be seen that the multiplicative noise enhances the low-frequency variability of anomalous SST variability by about 20% (even as the total noise variance increases only by about 8%). (b) The spectral densities ratios of the multiplcative noise models to the additive noise models.

a)

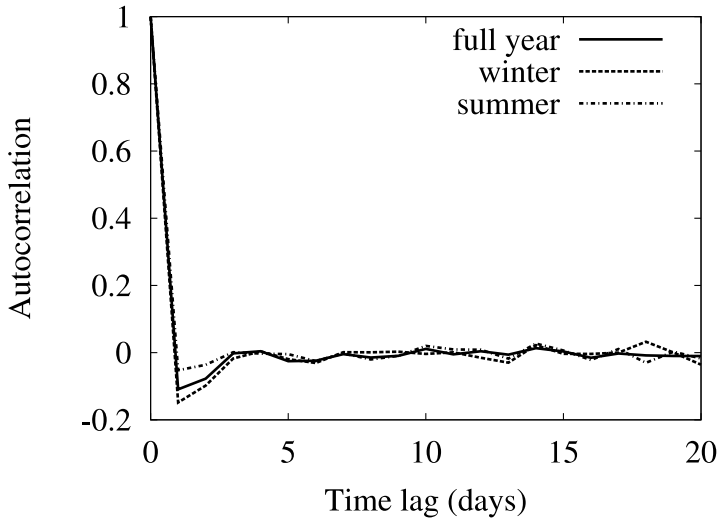

b)

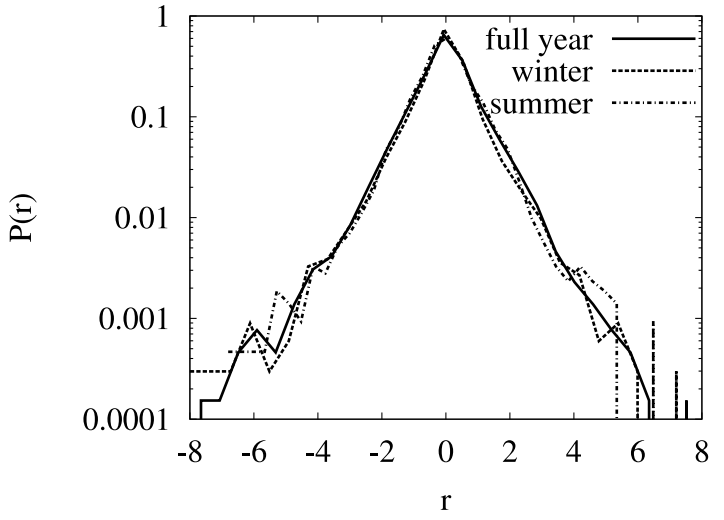

Figure 6: a) Autocorrelation function and b) PDF of the residual $r \equiv T'_{o\,Obs}(t + \Delta t) - T'_o(t + \Delta t)$ for the SST anomalies at OWS P. Note that the autocorrelation is close to zero after one time step (one day) and that the residual is highly non-Gaussian (very close to an exponential distribution).

a)

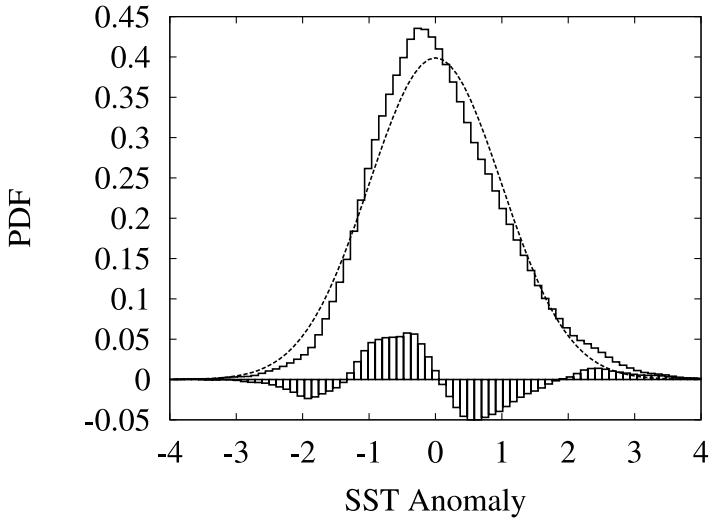

b)

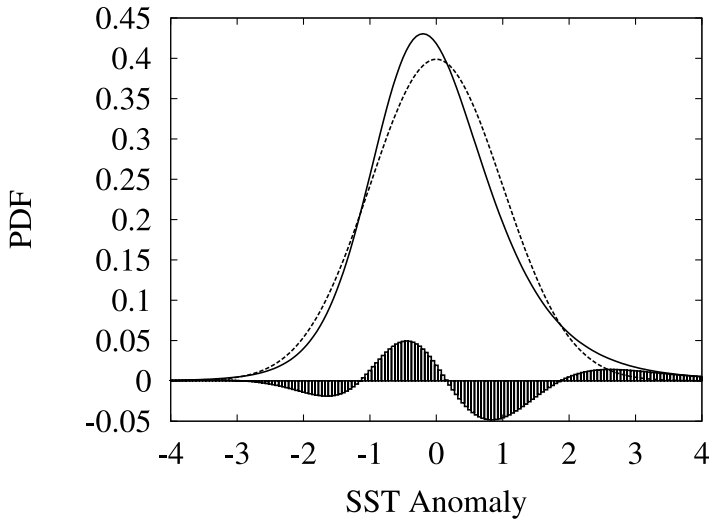

Figure 7: The PDFs of concatenated SST anomalies (nondimensional), related Gaussian distributions, and deviations from Gaussianity. In (a) the PDF (steps) is calculated as a normalized histogram. The dashed line is the related Gaussian distribution, whereas the boxes denote deviations from Gaussianity. Note that the PDF has a strong peak, weak flanks, and heavy tails relative to a Gaussian distribution (the PDF is kurtosed). Furthermore, the PDF is slightly skewed. In (b) the PDF (solid line) is calculated as a MLE to a skew t-distribution. The dashed line is the related Gaussian distribution, whereas the boxes denote deviations from Gaussianity.

a)

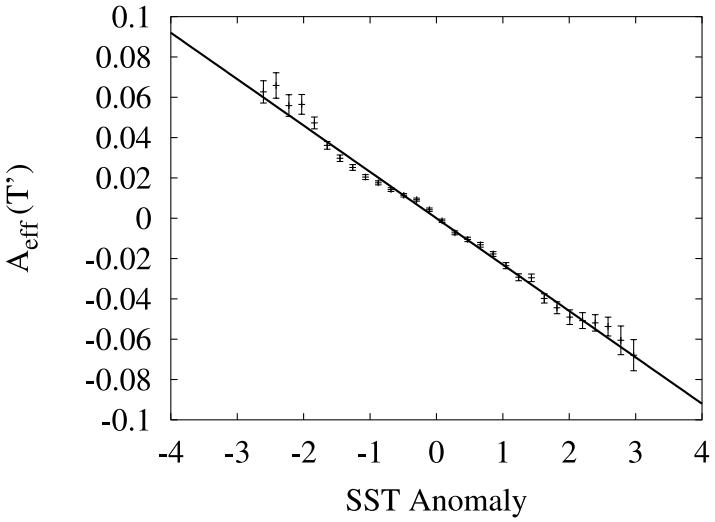

b)

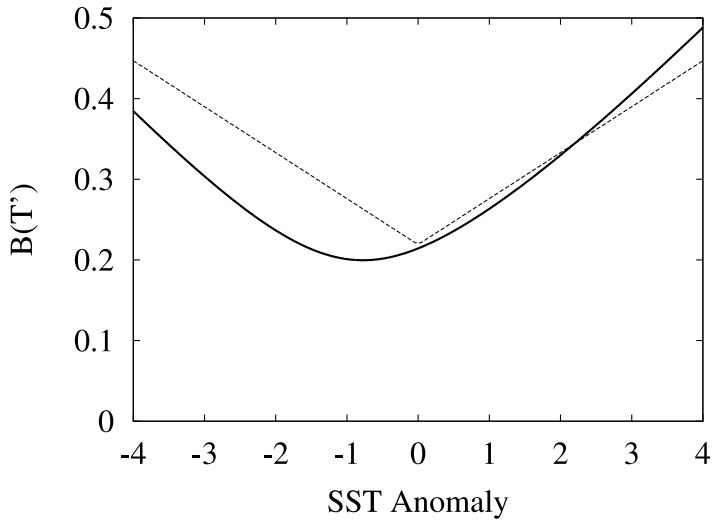

Figure 8: (a) The estimated effective drift $A_{eff}(T'_o)$ and (b) the estimated noise $B(T'_o)$ (in the figure $T'_o \equiv T'$) for the concatenated SST anomalies (nondimensional). The error bars in (a) indicate $\pm$ one standard error. The solid line in (a) shows the best linear fit. The dotted line in (b) shows the optimal linear multiplicative noise obtained by fitting the variance and the kurtosis of the PDF (Fig. 7) to the SDE (11).

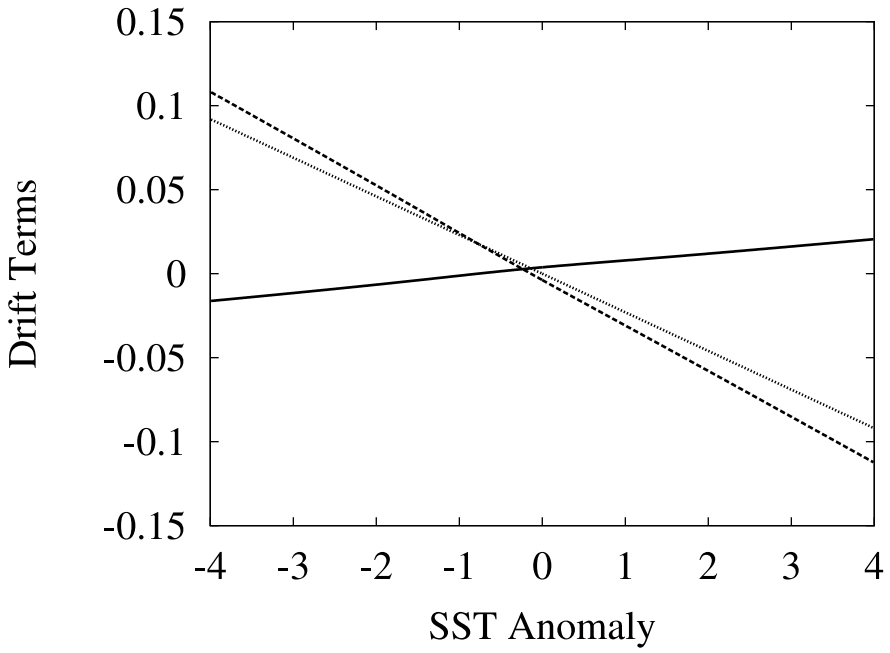

Figure 9: Noise-induced drift $1/2B(\partial B/\partial T_o')$ (solid line), deterministic drift A (dashed line), effective drift A_{eff} (dotted line) for the concatenated SST anomaly record.

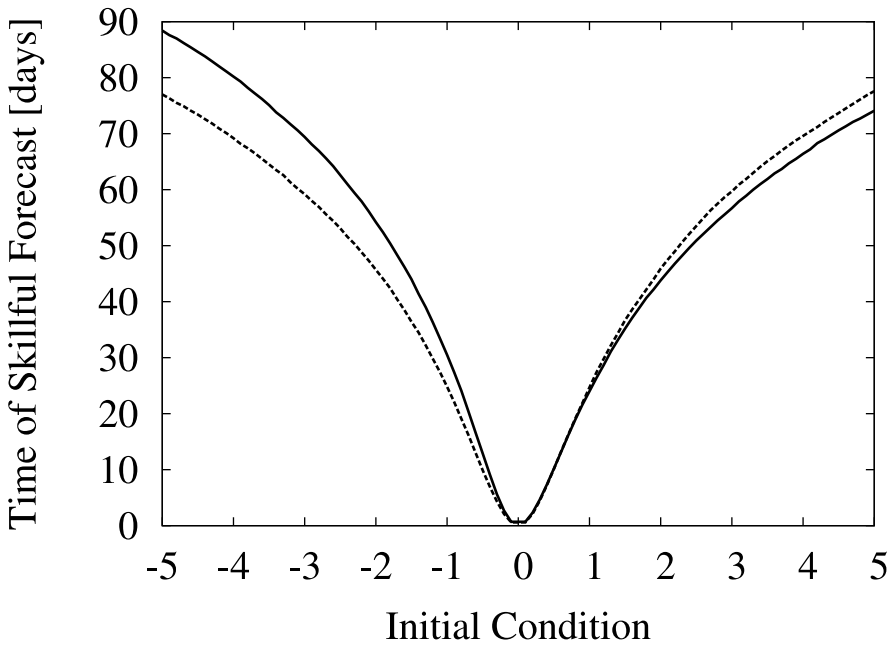

Figure 10: Time of skillful forecast (defined as $\rho_\infty = 0.5$) as a function of initial condition for the additive noise model (dashed line) and the multiplicative noise model (solid line).

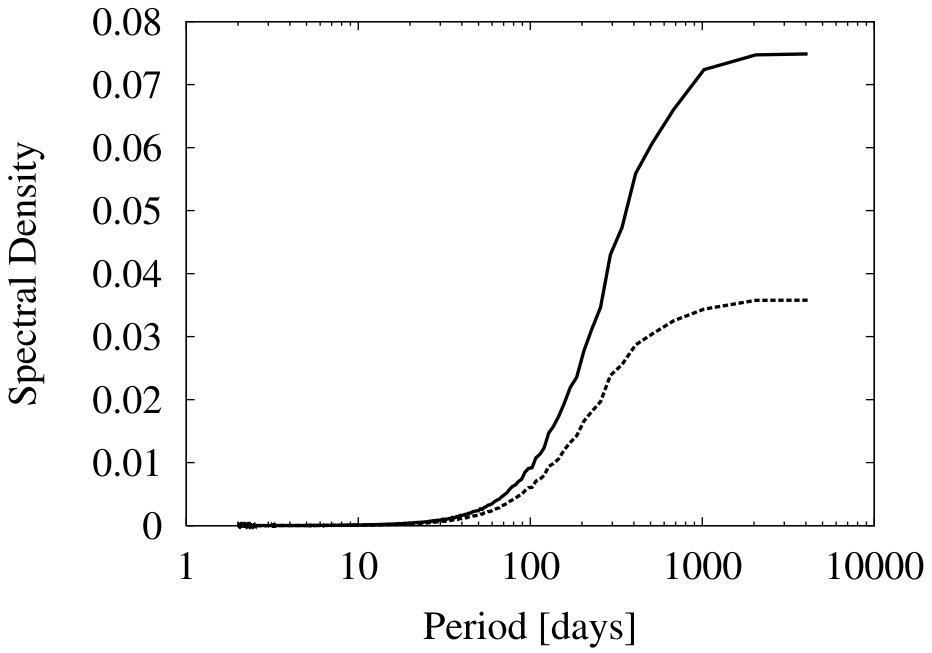

Figure 11: Spectra of nonlinearly modeled anomalous SST variability without and with muliplicative noise. The spectrum with pure additive noise is indicated by the dashed line, and the spectrum with multiplicative noise included is indicated by the solid line. It can be seen that the multiplicative noise enhances the low-frequency variability of anomalous SST variability by about 100% (even as the total noise variance increases only by about 30%).

a)

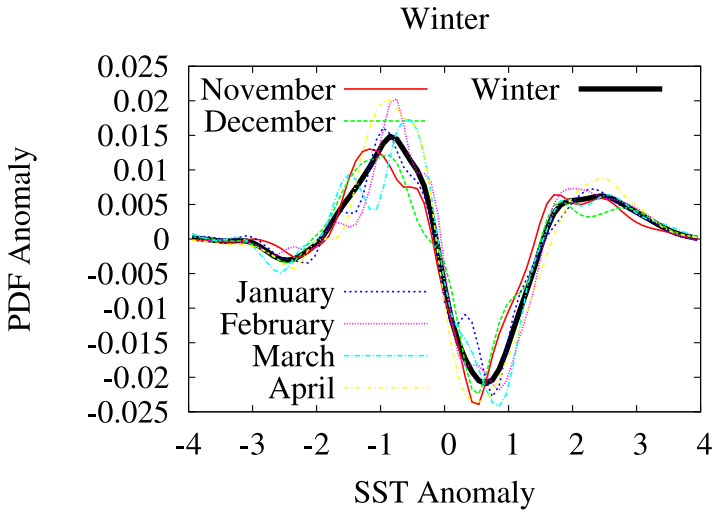

b)

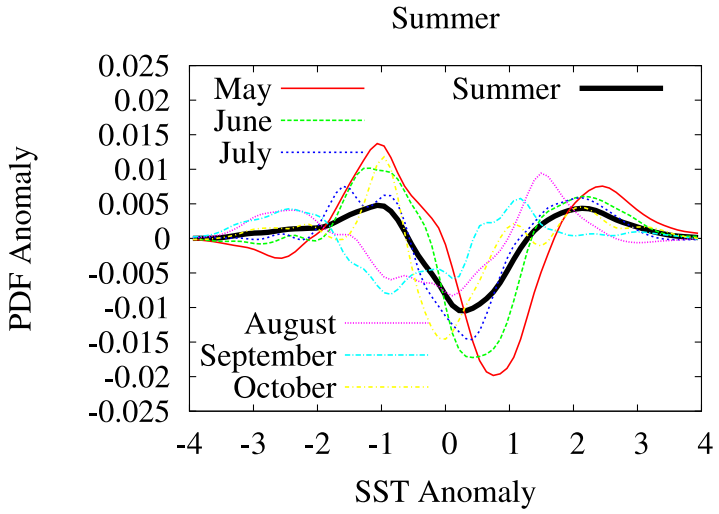

Figure 12: Monthly PDF anomalies of normalized daily SST anomalies for (a) extended winter (black solid line) and individual months (thin colored lines) and (b) for extended summer (black solid line) and individual months (thin colored lines) from the mixed layer model. The PDFs are calculated as normalized histograms.

a)

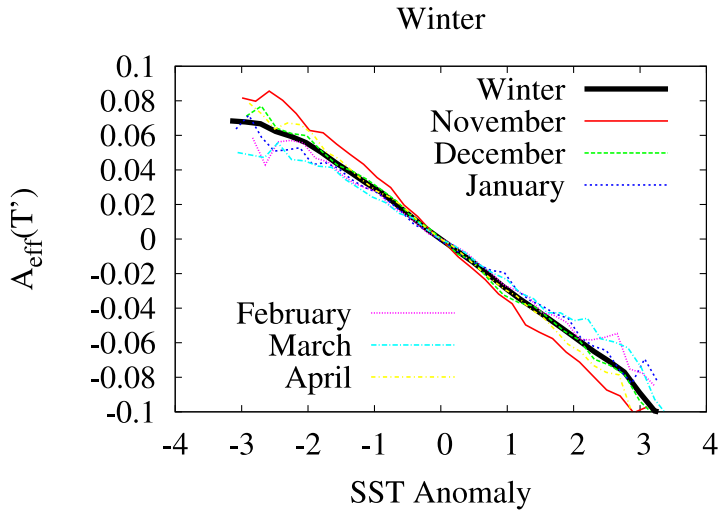

b)

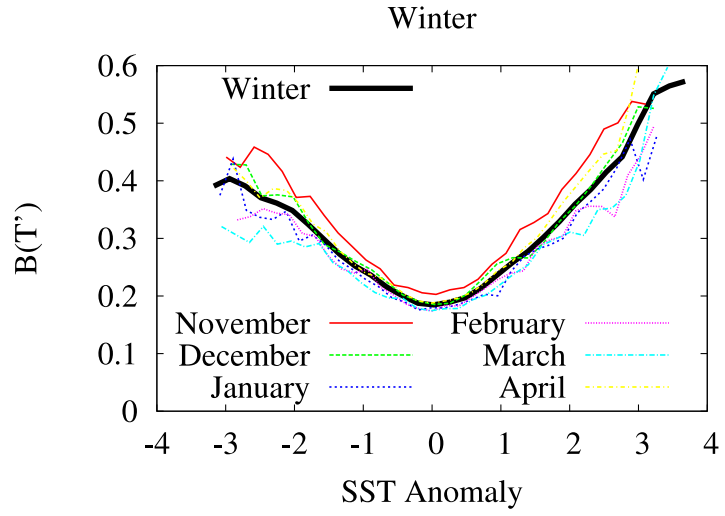

Figure 13: (a) The estimated effective drifts $A_{eff}(T'_o)$ and (b) the estimated noises $B(T'_o)$ (in the figure $T'_o \equiv T'$) of extended winter SST anomalies (thick black lines) and individual months (thin colored lines) from the mixed layer model.

a)

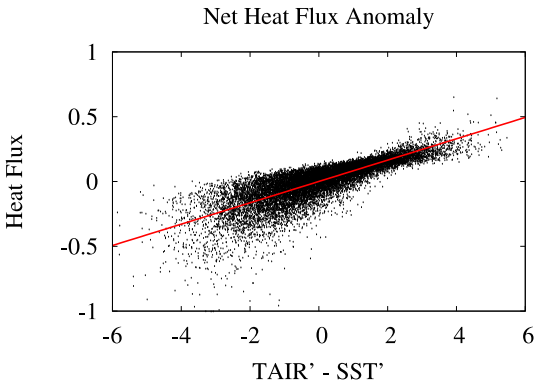

b)

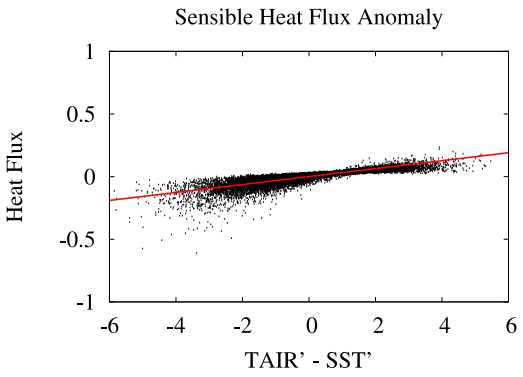

c)

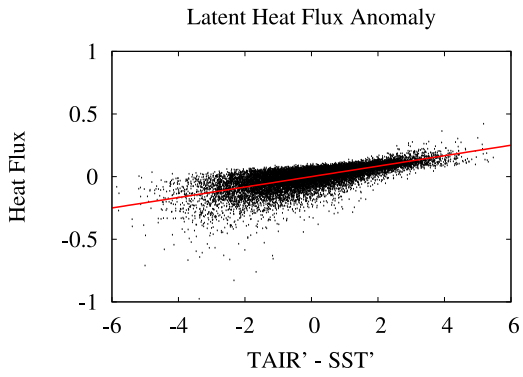

d)

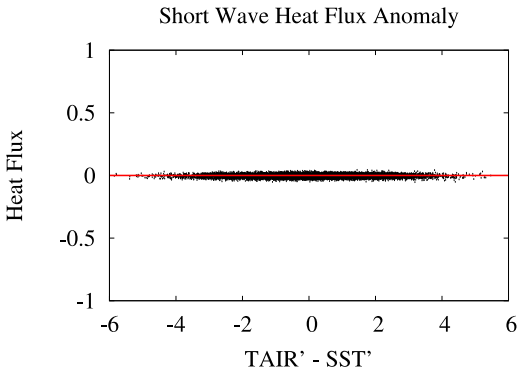

e)

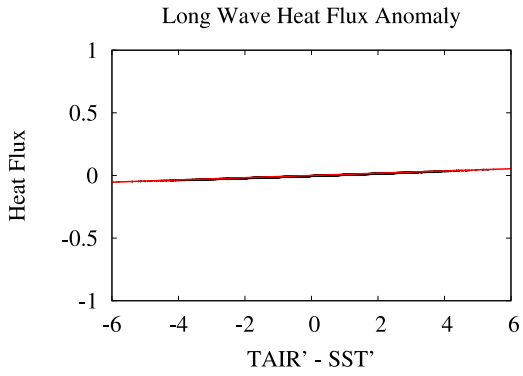

Figure 14: Scatter plots and the related linear fits of the following wintertime anomalous heat flux terms (in 10^{-6} K s^{-1}) from the mixed layer model as a function of the anomalous air-sea temperature difference (TAIR'-SST'): (a) anomalous net heat flux, (b) anomalous sensible heat flux, (c) anomalous latent heat flux, (d) anomalous short-wave radiation flux, (e) anomalous long-wave radiation flux (the scatter of the anomalous long-wave heat flux is so small that it is masked by the linear fit).